

Supplementary Information for:

Dominant Factors Limiting Optical Gain in Layered Two-Dimensional Halide Perovskite Thin Films†

Wee Kiang Chong^{a,b}, Krishnamoorthy Thirumal^{c,d}, David Giovanni^{a,b}, Teck Wee Goh^b, Xinfeng Liu^{b,e}, Nripan Mathews^{c,f}, Subodh Mhaisalkar^{*c,f}, and Tze Chien Sum^{*b}

^aEnergy Research Institute @ NTU, ERI@N, Interdisciplinary Graduate School, Nanyang Technological University, Singapore

^bDivision of Physics and Applied Physics, School of Physical and Mathematical Sciences, Nanyang Technological University, 21 Nanyang Link, Singapore 637371

^cEnergy Research Institute @NTU (ERI@N), Research Techno Plaza, X-Frontier Block, Level 5, 50 Nanyang Drive, Singapore 637553

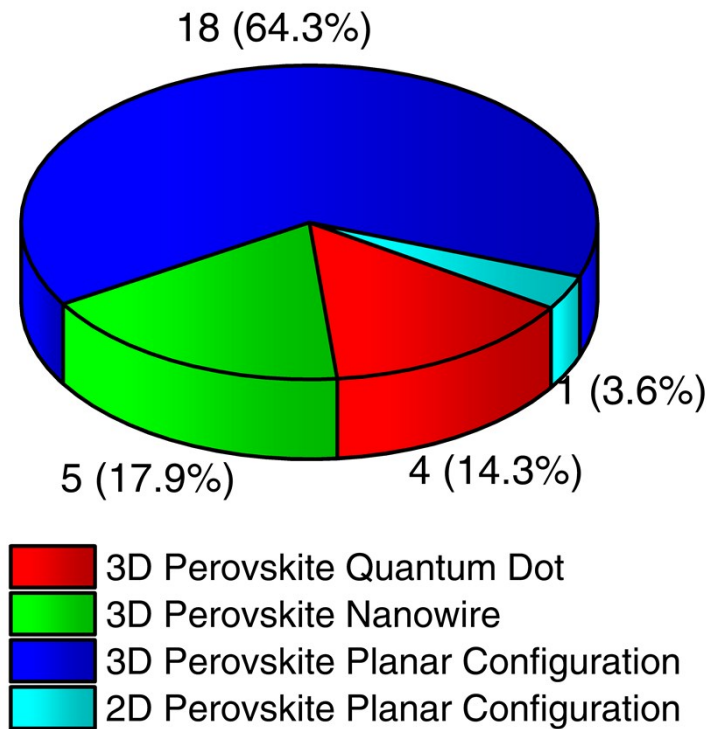
^dDivision of Chemistry and Biological Chemistry, School of Physical and Mathematical Sciences, Nanyang Technological University, 21 Nanyang Link, Singapore 637371

^eCAS Key Laboratory of Standardization and Measurement for Nanotechnology, National Center for Nanoscience and Technology, Beijing 100190, China

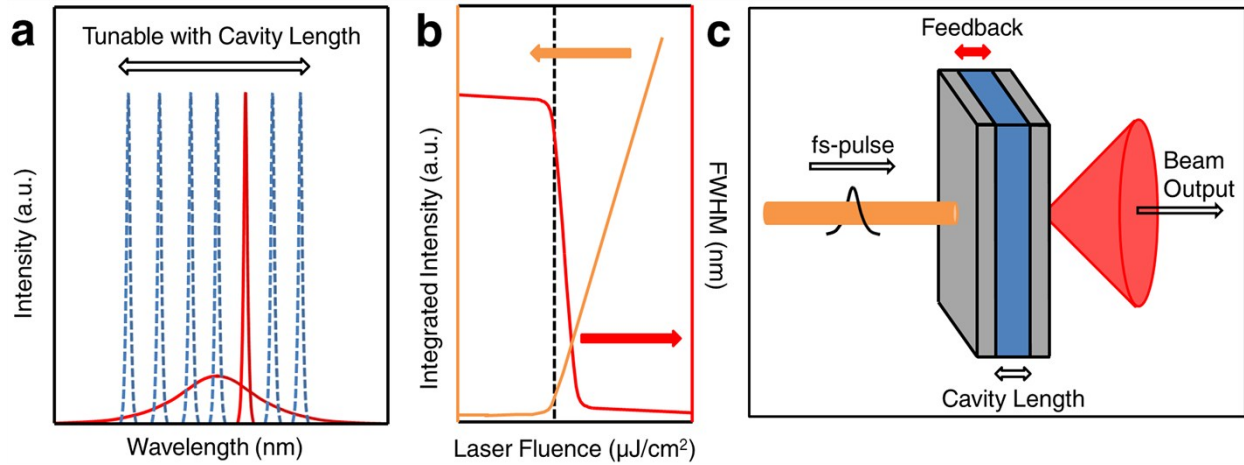
^fSchool of Materials Science and Engineering, Nanyang Technological University, Nanyang Avenue, Singapore 639798

*Corresponding Authors: T.C.S.: Tzechien@ntu.edu.sg; S.M.: Subodh@ntu.edu.sg

Perovskite optical gain reports
(1997- 3rd March 2016)

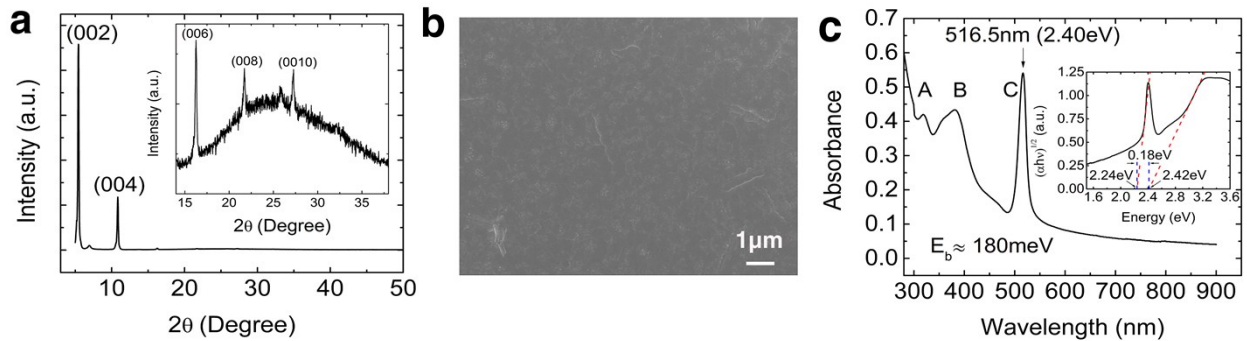


Supplementary Figure S1 | Disproportionate optical gain reports from 2D perovskite. Pie chart depicting the number of optical gain reports from 2D¹ and 3D perovskite²⁻²⁸. Till date, there is only one claim of lasing from 2D perovskite cavity structure.

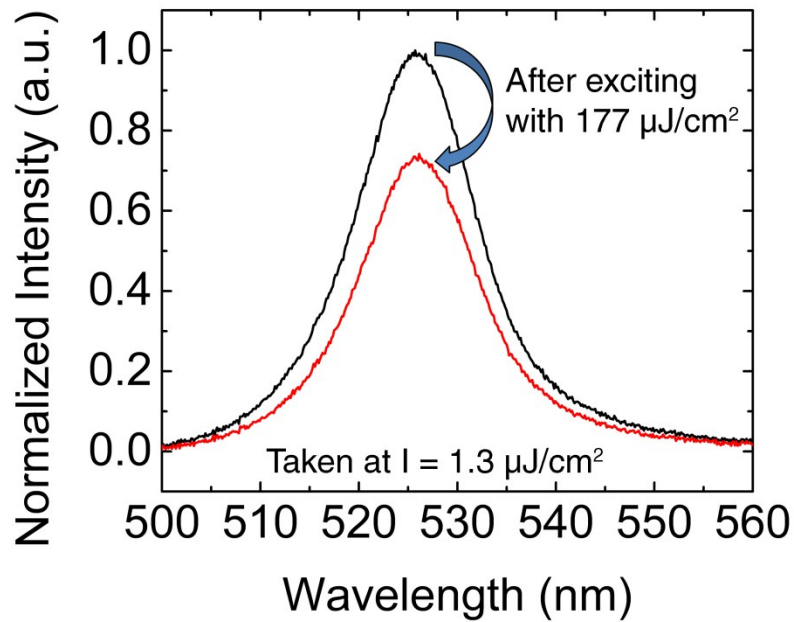


Supplementary Figure S2 | Characteristics of lasing phenomenon²⁹. **a**, Narrow emission linewidth with lasing wavelength dependent on cavity and gain medium. The gain bandwidth lies within the broad spontaneous emission region (condition 1 and 2). **b**, Threshold associated with integrated emission intensity and full width at half maximum (FWHM) (condition 3). **c**, Lasing output consists of a beam (condition 4).

X-ray Diffraction (XRD), Scanning Electron Microscopy (SEM) and Steady State absorption Characterization of PEPI. The XRD spectrum of the as-grown PEPI consists of periodic peaks with $\sim 5^\circ$ interval as shown in Fig. S3a. The periodic feature is representative of a layered structure and is typical for 2D perovskite³⁰. The SEM image revealed good substrate coverage and sample morphology – Fig 3b. A strong excitonic absorption peak at 2.40 eV can also be observed - Fig. S3c. From the Tauc plot, the material bandgap and excitonic band edge energy was estimated to be 2.42 eV and 2.24 eV respectively – Fig S3c inset. Taking the difference between these energy values, an exciton binding energy of ~ 180 meV can be obtained. This is consistent with several literatures³¹⁻³³ and is typical for the excitonic 2D perovskite system.

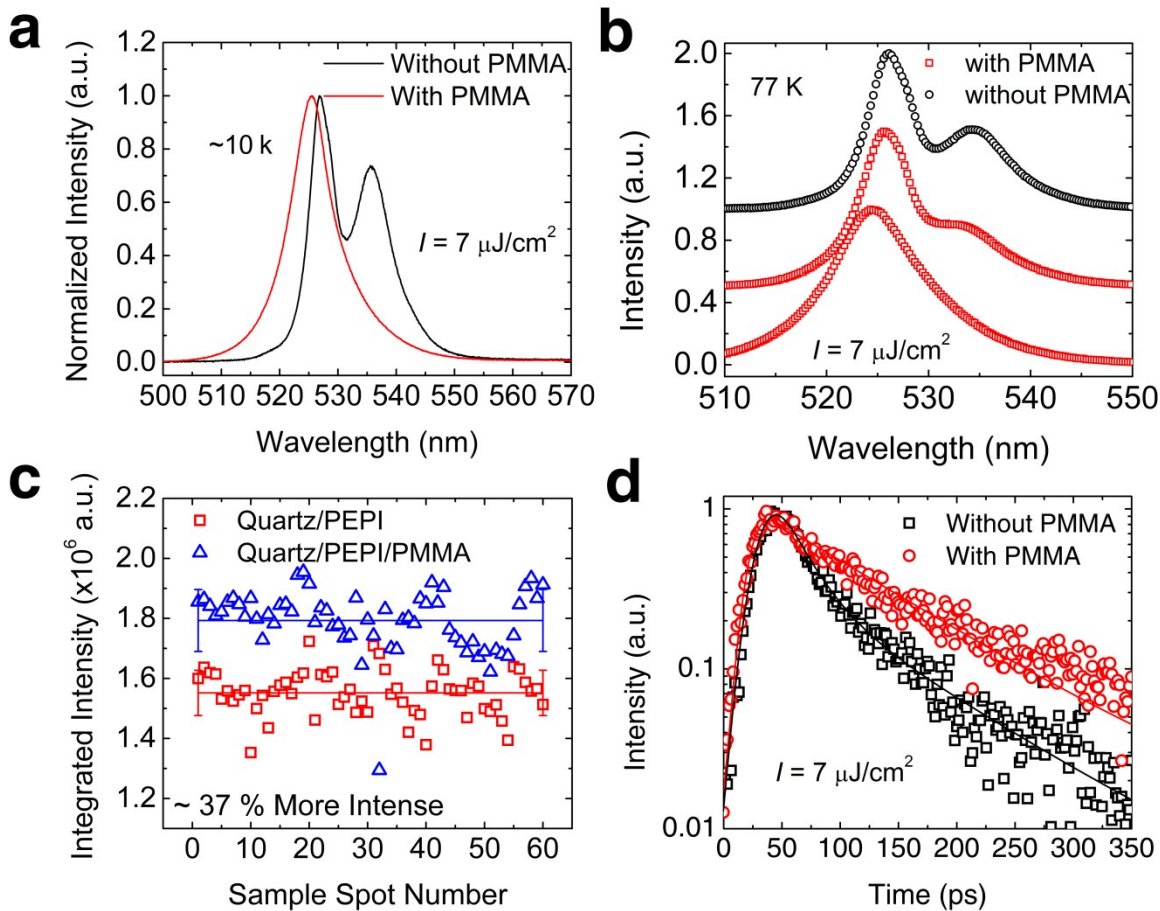


Supplementary Figure S3 | Physical characterizations of PEPI. **a**, XRD spectrum of PEPI. Inset shows the magnified smaller periodic diffraction peaks. The broad peak center at 25° corresponds to the quartz substrate peak. **b**, SEM image of PEPI thin film showing good substrate coverage and sample morphology. **c**, Room temperature steady state absorption spectrum of PEPI. A sharp exciton absorption peak is observed at 516.5nm. Peaks at ~ 325 nm and ~ 400 nm corresponds to transition from Pb 6s and I 5p hybridization orbital to Pb 6P orbital³². Inset shows the estimation of the exciton binding energy.



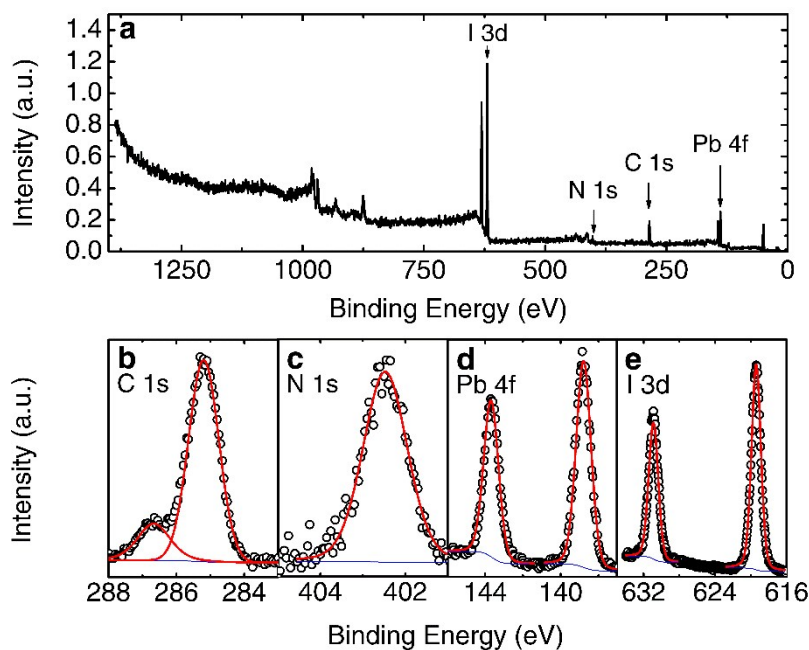
Supplementary Figure S4 | Effects of high laser fluence on low laser fluence PL spectrum.

Steady-state PL spectrum of PEPI excited with 400nm, taken at pump fluence of $1.3 \mu\text{J}/\text{cm}^2$, before and after exposure to high laser fluence of $177 \mu\text{J}/\text{cm}^2$. The damage threshold is defined here to be the laser fluence that reduces the PL intensity. Typical damage fluence found in PEPI is of the order of $100\mu\text{J}/\text{cm}^2$.



Supplementary Figure S5 | Effects of PMMA overlayer on PEPI PL emission. **a**, 10 K PL spectrum of PEPI with and without PMMA layer. Peak 2 is observed to quench significantly after PMMA deposition. **b**, 77 K PL spectrum of PEPI with and without PMMA layer. The degree of quenching from peak 2 was found vary among samples. This suggests that the origin of peak 2 could be related to both bulk and surface effect. **c**, Integrated PL intensity of PEPI with and without PMMA taken at 60 equally distributed sample spot across a $\sim 0.75 \times 0.75 \text{ cm}^2$ sample area. The average and standard distribution are also included. Time resolved PL spectrum of peak 1 with and without PMMA. There is a lifetime lengthening of peak 1 with PMMA is consistent with trap passivation. All experiments were conducted using 400 nm pulse excitation and laser fluence of $7 \mu\text{J}/\text{cm}^2$.

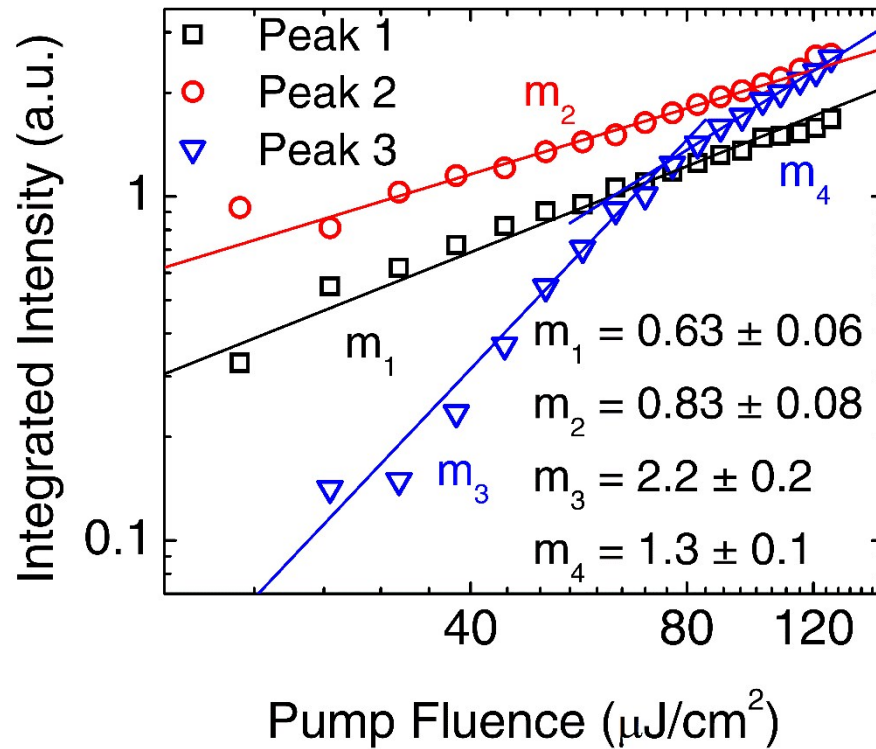
X-ray Photoelectron Spectroscopy (XPS) Studies. XPS study is employed to investigate the surface elemental composition of the perovskite since a large surface contribution has been found from peak 2. Supplementary Figure S6 (a) shows the XPS wide scan of PEPI film while figure (b), (c) and (d) shows the narrow scan of the respective C 1s, N 1s, Pb 4f and I 3d peaks. Supplementary Table S1 shows the surface elemental ratio of the perovskite obtained from the integrated area of the narrow scan. The results indicate that the surface contains organic vacancies, which could be responsible for peak 2 emission. The presence of small activation energy of 10 meV (see Figure 2) could arise from the energy barrier between the free exciton state and this vacancy state. Therefore, the occupancy of this vacancy state is likely due to transfer from free exciton state (peak 1).



Supplementary Figure S6 | XPS elemental peaks characterization of PEPI. a, XPS wide scan of PEPI with respective elements labeled. XPS narrow scan of the respective elemental peaks: (b) C 1s, (c) N 1s, (d) Pb 4f and (e) I 3d.

Supplementary Table S1 | Organic deficiency at PEPI surface. The surface elemental composition ratio is derived from the area under the respective XPS narrow scan curve in Figure S6 (b) to (e). The element C and N were found to be lesser than the ideal case.

Element	C	N	Pb	I
Stoichiometric Ratio	16	2	1	4
XPS Results	11.2	1.7	1.0	4.0

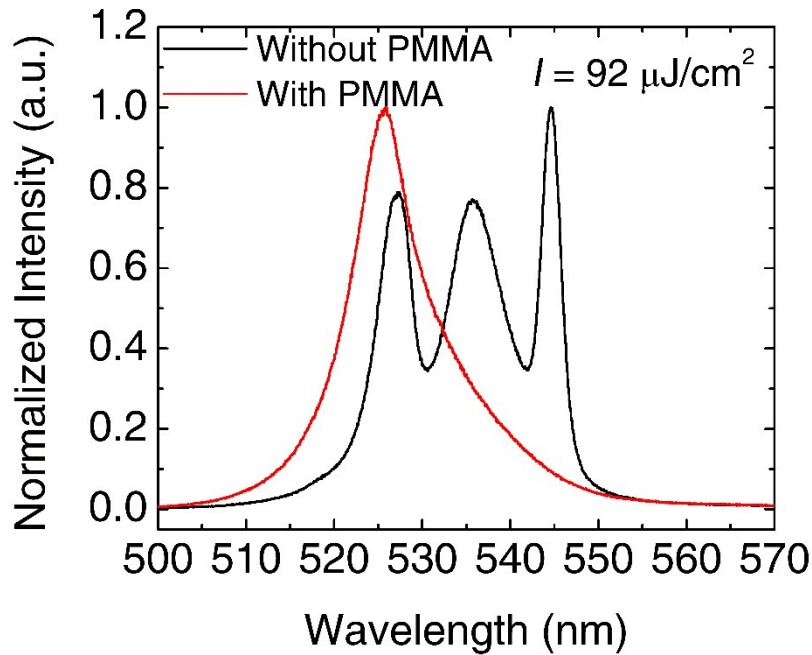


Supplementary Figure S7 | Origins of peak 3. Plot of integrated PL intensity with pump fluence. The integrated PL intensity of the respective peaks is fitted with power law ($y_i = k_i x^{m_i}$). The exponent m_i indicates the behavior of the respective species under different pump fluence. The value of m_3 for peak 3 is approximately twice compared to m_1 and m_2 for peak 1 and 2 respectively which suggests a biexcitonic origin. The reduction of m_3 to m_4 at higher laser fluence is likely due to exciton-biexciton scattering³⁴. The experiment were conducted using 400 nm pulse excitation of pristine PEPI thin film.

PEPI biexciton binding energy determination. The biexciton binding energy (E_b) is defined as

$$E_b = 2E_x - E_{xx} = E_x - (E_{xx} - E_x) \quad (\text{S1})$$

where E_x is the exciton energy and E_{xx} is the biexciton energy. For PEPI, E_x corresponds to the bound exciton energy (peak 2). The radiative recombination of a biexciton involves a photon emission and an exciton formation. The photon emitted gives rise to the observed peak 3. Therefore, the biexciton binding energy is the energy difference between peak 3 and peak 2.



Supplementary Figure S8 | Significant quenching of biexciton emission. High laser fluence ($\sim 92 \mu\text{J}/\text{cm}^2$) PL spectrum excited with and without PMMA overlayer. Peak 3 is observed to be quenched significantly after PMMA addition. The experiment was conducted using 400 nm pulse laser.

Supplementary Table S2. Parameters for the rate equations.

Parameter	Meaning	Value
$\hbar\omega$	Pump photon energy.	3.1 eV
α	Absorption coefficient at pump energy.	$2.086 \times 10^5 \text{ cm}^{-1}$
τ_{Xr}	Exciton radiative lifetime.	100 ps
k_{Xnr}	Exciton non-radiative relaxation rate.	0.011 ps^{-1}
$\tau_{X_B^r}$	Bound exciton non-radiative relaxation rate.	150 ps
$k_{X_B^{nr}}$	Bound biexciton non-radiative relaxation rate.	0.04 ps^{-1}
τ_{XXr}	Bound biexciton Radiative relaxation rate.	50 ps
D_X	Density of states	$4 \times 10^{21} \text{ cm}^{-3}$
τ_{CX}	Free carrier to exciton relaxation time	50 fs
τ_{CX_B}	Free carrier to bound exciton relaxation time	10 fs
τ_L	Laser time constant	100 fs
C_X	Bound exciton trapping	9 ns^{-1}
B_{XX_B}	Bound biexciton formation coefficient	$8 \times 10^{-21} \text{ cm}^3$
γ	Exciton-exciton annihilation coefficient	$3.38 \times 10^{-12} \text{ cm}^3/\text{s}$
v_{gX}	Group velocity at exciton emission energy	$1.14 \times 10^8 \text{ m/s}$
v_{gX_B}	Group velocity at bound exciton emission energy	$1.25 \times 10^8 \text{ m/s}$
v_{gXX_B}	Group velocity at bound biexciton emission energy	$1.31 \times 10^8 \text{ m/s}$
g_X	Exciton optical gain	$1.038 \times 10^5 \text{ cm}^{-1}$
g_{X_B}	Bound exciton optical gain	$6.603 \times 10^4 \text{ cm}^{-1}$
g_{XX_B}	Bound biexciton optical gain	$4.964 \times 10^4 \text{ cm}^{-1}$

References:

1. T. Kondo, T. Azuma, T. Yuasa and R. Ito, *Solid State Commun.*, 1998, **105**, 253-255.
2. J. Pan, S. P. Sarmah, B. Murali, I. Dursun, W. Peng, M. R. Parida, J. Liu, L. Sinatra, N. Alyami, C. Zhao and others, *J. Phys. Chem. Lett.*, 2015.
3. Y. Wang, X. Li, J. Song, L. Xiao, H. Zeng and H. Sun, *Adv. Mater.*, 2015, **27**, 7101-7108.
4. S. Yakunin, L. Protesescu, F. Krieg, M. I. Bodnarchuk, G. Nedelcu, M. Humer, G. De Luca, M. Fiebig, W. Heiss and M. V. Kovalenko, *Nat. Commun.*, 2015, **6**.
5. Y. Xu, Q. Chen, C. Zhang, R. Wang, H. Wu, X. Zhang, G. Xing, W. W. Yu, X. Wang and Y. Zhang, *J. Am. Chem. Soc.*, 2016.
6. K. Wang, Z. Gu, S. Liu, J. Li, S. Xiao and Q. Song, *Opt. Lett.*, 2016, **41**, 555-558.
7. S. W. Eaton, M. Lai, N. A. Gibson, A. B. Wong, L. Dou, J. Ma, L.-W. Wang, S. R. Leone and P. Yang, *Proc. Natl. Acad. Sci. USA*, 2016, **113**, 1993-1998.
8. H. Zhu, Y. Fu, F. Meng, X. Wu, Z. Gong, Q. Ding, M. V. Gustafsson, M. T. Trinh, S. Jin and X. Y. Zhu, *Nat. Mater.*, 2015, **14**, 636-642.
9. Y. Fu, H. Zhu, A. W. Schrader, D. Liang, Q. Ding, P. Joshi, L. Hwang, X. Y. Zhu and S. Jin, *Nano Lett.*, 2016, **16**, 1000-1008.
10. M. Cadelano, V. Sarritzu, N. Sestu, D. Marongiu, F. Chen, R. Piras, R. Corpino, C. M. Carbonaro, F. Quochi, M. Saba and others, *Adv. Opt. Mater.*, 2015, **3**, 1557-1564.
11. B. R. Sutherland, S. Hoogland, M. M. Adachi, C. T. O. Wong and E. H. Sargent, *ACS Nano*, 2014, **8**, 10947-10952.
12. K. Chen, A. J. Barker, F. L. C. Morgan, J. E. Halpert and J. M. Hodgkiss, *J. Phys. Chem. Lett.*, 2014, **6**, 153-158.
13. L. Qin, L. Lv, Y. Ning, C. Li, Q. Lu, L. Zhu, Y. Hu, Z. Lou, F. Teng and Y. Hou, *RSC Adv.*, 2015, **5**, 103674-103679.
14. S. D. Stranks, S. M. Wood, K. Wojciechowski, F. Deschler, M. Saliba, H. Khandelwal, J. B. Patel, S. Elston, L. M. Herz, M. B. Johnston and others, *Nano Lett.*, 2015.
15. F. Deschler, M. Price, S. Pathak, L. E. Klintberg, D.-D. Jarausch, R. Higler, S. Hüttner, T. Leijtens, S. D. Stranks, H. J. Snaith and others, *J. Phys. Chem. Lett.*, 2014, **5**, 1421-1426.
16. T. S. Kao, Y.-H. Chou, C.-H. Chou, F.-C. Chen and T.-C. Lu, *Appl. Phys. Lett.*, 2014, **105**, 231108-231108.
17. G. Xing, N. Mathews, S. S. Lim, N. Yantara, X. Liu, D. Sabba, M. Grätzel, S. Mhaisalkar and T. C. Sum, *Nat. Mater.*, 2014, **13**, 476-480.
18. Y. Wang, X. Li, X. Zhao, L. Xiao, H. Zeng and H. Sun, *Nano Lett.*, 2015.
19. Y. J. Li, Y. Lv, C.-L. Zou, W. Zhang, J. Yao and Y. S. Zhao, *J. Am. Chem. Soc.*, 2016, **138**, 2122-2125.
20. Q. Liao, K. Hu, H. Zhang, X. Wang, J. Yao and H. Fu, *Adv. Mater.*, 2015.
21. N. Arora, M. I. Dar, M. Hezam, W. Tress, G. Jacopin, T. Moehl, P. Gao, A. S. Aldwayyan, B. Deveaud, M. Grätzel and M. K. Nazeeruddin, *Adv. Funct. Mater.*, 2016, DOI: 10.1002/adfm.201504977, n/a-n/a.
22. I. Suárez, E. J. Juárez-Pérez, J. Bisquert, I. Mora-Seró and J. P. Martínez-Pastor, *Adv. Mater.*, 2015, **27**, 6157-6162.
23. R. Dhanker, A. N. Brigeman, A. V. Larsen, R. J. Stewart, J. B. Asbury and N. C. Giebink, *Appl. Phys. Lett.*, 2014, **105**, 151112-151112.

24. D. Priante, I. Dursun, M. S. Alias, D. Shi, V. A. Melnikov, T. K. Ng, O. F. Mohammed, O. M. Bakr and B. S. Ooi, *Appl. Phys. Lett.*, 2015, **106**, 081902-081902.
25. Q. Zhang, S. T. Ha, X. Liu, T. C. Sum and Q. Xiong, *Nano Lett.*, 2014, **14**, 5995-6001.
26. M. Saliba, S. M. Wood, J. B. Patel, P. K. Nayak, J. Huang, J. A. Alexander-Webber, B. Wenger, S. D. Stranks, M. T. Hörantner, J. T.-W. Wang and others, *Adv. Mater.*, 2015.
27. J. Xing, X. F. Liu, Q. Zhang, S. T. Ha, Y. W. Yuan, C. Shen, T. C. Sum and Q. Xiong, *Nano Lett.*, 2015, **15**, 4571-4577.
28. Z. Gu, K. Wang, W. Sun, J. Li, S. Liu, Q. Song and S. Xiao, *Adv. Opt. Mater.*, 2016, **4**, 472-479.
29. I. D. W. Samuel, E. B. Namdas and G. A. Turnbull, *Nature Photon.*, 2009, **3**, 546-549.
30. K. Pradeesh, K. N. Rao and G. V. Prakash, *J. Appl. Phys.*, 2013, **113**, 083523.
31. K. Gauthron, J. Lauret, L. Doyennette, G. Lanty, A. Al Choueiry, S. Zhang, A. Brehier, L. Largeau, O. Mauguin and J. Bloch, *Opt. Express*, 2010, **18**, 5912-5919.
32. N. Kitazawa, M. Aono and Y. Watanabe, *Mater. Chem. Phys.*, 2012, **134**, 875-880.
33. X. Hong, T. Ishihara and A. V. Nurmikko, *Phys. Rev. B*, 1992, **45**, 6961.
34. C. Benoit À La Guillaume, F. Salvan and M. Voos, *JOL*, 1970, **1**, 315-323.